Michiel Postema*, Christine Gering, Nicole Anderton, Craig S. Carlson, and Minna Kellomäki

Monitoring the gelation of gellan gum with torsion rheometry and brightness-mode ultrasound

https://doi.org/10.1515/cdbme-2022-1010

Abstract: Gellan gum is a hydrogel with several applications in ultrasonic imaging, novel drug delivery, and tissue regeneration. As hydrogels are dynamic entities, their viscocelastic and therefore their acoustic properties change over time, which is of interest to monitor. To determine the speed of sound from brightness-mode images, however, rather large quantities of hydrogel are needed. In this study, we investigated torsion rheometry as a means to determine acoustic properties. Perceived speeds of sound were derived and computed from torsion rheometry measurements of gelating gellan gum mixed with spermidine trihydrochloride crosslinker. For comparison, brightness-mode ultrasonic images were recorded of the same material inside a phantom well. The rheometry data converged to a speed of sound within a standard devitation of the speed of sound measured from the brightness-mode images. We have shown that dynamic acoustic properties of gelating gellan gum can be simulated and experimentally determined using torsion rheometry.

Keywords: Hydrogel gelation, shear modulus, dynamic modulus, acoustic imaging, B-mode, Zener model, perceived speed of sound, rheometry.

1 Introduction

Biocompatible hydrogels have been under investigation for their role as tissue-mimicking phantoms, artificial cell niches, and drug delivery vehicles [1–3]. An example of such a biocompatible hydrogel is gellan gum, a strong and thermally stable polysaccharide gel [4]. Gellan gum has been used in medical applications including cell culturing [5–8], imaging [4], drug delivery [9], and tissue regeneration [10].

Gellan gum forms self-supporting hydrogels in the presence of cations [11]. During the sol–gel transition generally referred to as gelation, crosslinking agents couple polymer chains to form a three-dimensional network via radical, chemical, or physical reactions [12]. Gelation increases both the elasticity and the dynamic viscosity of hydrogels over time [1]. This process may be accelerated or decelerated by external factors, including temperature and sound [13], and may even be inverted [14].

Real-time gelation monitoring is crucial in the development of novel hydrogel applications. The measurement of the gelation process is done by means of dynamic testing, *e.g.*, with a rotating-plate rheometry setup, through which the dynamic moduli are determined [15]. Reliable outcomes of rheology experiments require less than a mL of testing material. However, the outcomes of rheology experiments have not been directly related to acoustics parameters. As a hydrogel does not solely exist in one phase, and as it is inherently dynamic in its viscous and elastic properties, it is not straightforward how to relate the moduli measured to the speed of sound. Conversely, ultrasonic imaging is rather straightforward, but inherently requires substantially larger quantities of near-homogenous material, whilst small testing quantities result in notoriously inaccurate measurements. In addition to measuring acoustic propagation, it has been of interest to determine whether the gelation process can be monitored using diagnostic ultrasound.

In this study, we monitored the gelation of gellan gum using diagnostic brighness-mode ultrasonic imaging. From these images, we measured the speed of sound in gellan gum as a function of time. This outcome was compared to the time-dependent speed computed from rotating-plate rheometry experiments.

***Corresponding author: Michiel Postema,** BioMediTech, Faculty of Medicine and Health Technology, Tampere University, Korkeakoulunkatu 3, 33720 Tampere, Finland and School of Electrical and Information Engineering, University of the Witwatersrand, Johannesburg, 1 Jan Smutslaan, Braamfontein 2050, South Africa, e-mail: michiel.postema@tuni.fi
Christine Gering, Nicole Anderton, Minna Kellomäki, BioMediTech, Faculty of Medicine and Health Technology, Tampere University, Tampere, Finland
Craig S. Carlson, BioMediTech, Faculty of Medicine and Health Technology, Tampere University, Tampere, Finland and School of Electrical Engineering, University of the Witwatersrand, Johannesburg, Braamfontein, South Africa

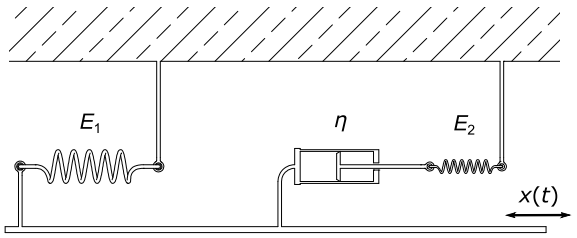

Fig. 1: Maxwell representation of a Zener model of an isotropic hydrogel, adapted for shear strain and subjected to a periodic displacement function $x(t)$.

2 Theory

Let us consider an isotropic hydrogel undergoing periodic shear displacement, whose Zener model is schematically shown in Figure 1, similar to [16]. The displacement driving function has the form $x(t) = A \sin \omega t$, where A is the displacement amplitude and ω is the angular displacement frequency. The Maxwell representation of the Zener model separates a storage component with elasticity E_1 from a loss component with dynamic viscosity η. For a hydrogel under consideration here, the resistance to plastic deformation, E_2, abides $E_2 \ll E_1$.

Choosing a fixed phase angle in the oscillation cycle, we can define a storage modulus function

$$G'(t) = E_1 \left(1 - e^{-\frac{E_2}{\eta} t}\right) \tag{1}$$

and a loss modulus function

$$G''(t) = \eta\, \omega \left(1 - e^{-\frac{E_2}{\eta} t}\right) . \tag{2}$$

Combining the storage and loss moduli yields the dynamic modulus G^*, whose magnitude is given by [17]

$$|G^*(t)| = \sqrt{G'(t)^2 + G''(t)^2} . \tag{3}$$

If the hydrogel is not gelating or not gelating anymore, no crosslinking of polymers takes place, resulting in the dynamic modulus to converge to the static shear modulus $G(t = \infty)$.

If the medium is isotropic and homogeneous, and if Poisson's ratio ν approximates 0.5, we may assume that Young's modulus equals $3G$ [17], and therefore

$$c(t) = \sqrt{\frac{2\,G(t)\,(1+\nu)}{\rho}} \approx \sqrt{\frac{3\,G(t)}{\rho}} , \tag{4}$$

where $c(t)$ is the speed of sound of the hydrogel and ρ is the density of the hydrogel [18]. It should be noted, that the dynamic modulus itself cannot simply be related to acoustic parameters, unless $t = \infty$. In this study, however, we define a perceived speed of sound $\mathfrak{c}(t)$ based on the dynamic modulus,

$$\mathfrak{c}(t) = \sqrt{\frac{3\,|G^*(t)|}{\rho}} , \tag{5}$$

which converges to the actual speed of sound at $t = \infty$:

$$\lim_{t\to\infty} \mathfrak{c}(t) = \lim_{t\to\infty} c(t) . \tag{6}$$

3 Materials and methods

3.1 Gellan gum preparation

The materials for gellan gum preparation were acquired from Merck KGaA (Darmstadt, Germany) unless stated otherwise. G1910 Gelzan™ CM Gelrite (low acyl, $M_w = 10^3\,\mathrm{kg\,mol^{-1}}$) was dissolved at 0.5% w/v in HEPES/sucrose (25 mM, 10% w/v sucrose, pH 6.5) buffer at 50°C for 30 min. This gellan gum solution was stored at 4°C but warmed to 37°C prior to experiments. Henceforth, we refer to this polymer solution as hydrogel precursor. For crosslinking, solutions of spermidine trihydrochloride (2 mM in HEPES/sucrose) was used in a 1:5 ratio of crosslinker to gellan gum.

3.2 Phantom preparation

An ultrasound phantom of dimensions $80.0 \times 80.0 \times 39.9\,\mathrm{mm^3}$ was produced as previously published [19], using Finax Psyllium 85% kostfiber (Abdon Food AB, Helsingborg, Sweden) instead of psyllium husk powder. Before pouring and cooling the phantom material, a $15.8 \times 15.8 \times 39.9\text{-mm}^3$ cuboid well was created with its proximal side at a distance of 32.2 mm from the front plane of the phantom. Prior to ultrasonic imaging experiments, the well was filled with prepared water ($c = 1480\,\mathrm{m\,s^{-1}}$) for calibration, emptied, and subsequently filled with gellan gum. The speed of sound of the phantom at experimenting temperature was measured to be $1501 \pm 110\,\mathrm{m\,s^{-1}}$.

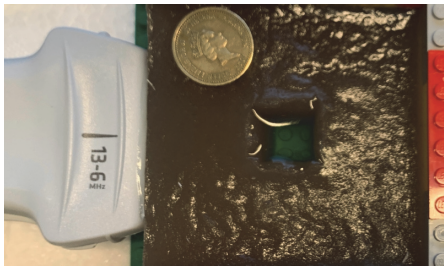

Fig. 2: Top view of the position of the ultrasound probe with respect to the phantom and the cuboid well filled with optically transparent hydrogel. A 1-SHP coin has been added for scale.

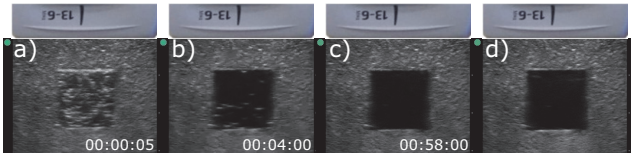

Fig. 3: Brightness-mode images of the cross-section of a cuboid well filled with gelating gellan gum at selected times (a–c) and a control with prepared water (d).

3.3 Ultrasonic imaging

An HFL38x 13–6-MHz linear probe of a SonoSite® M-Turbo® sonography device (Fujifilm Sonosite, Inc., Bothell, WA, USA) was positioned in horizontal orientation with its surface touching the front plane of the phantom, such that the cross-section of the well was in the central field of view of the probe, as shown in Figure 2. The sonography device was operating in musculoskeletal pulsed brightness mode with a penetration depth of 60 mm relative to the probe surface. Ultrasound pulses were indicated to have a mechanical index of 0.6 and a thermal index of 0.1. The machine settings remained unaltered throughout the experiments.

A still frame was captured immediately after well filling. The gellan gum poured was allowed to settle for four minutes, after which video clip recording commenced. Brightness-mode video clips were collected continuously during the subsequent 18 minutes. Thereafter, a brightness-mode still frame was collected every five minutes.

3.4 Rheometry

Rheological time sweep experiments were performed with a DHR-2 hybrid rheometer (TA Intruments, New Castle, DE, USA) in torsion mode. For each torsion experiment, 400 μL hydrogel was pipetted on the bottom plate of the rheometer, after which the gap between plate and geometry was lessened to 1500 μm. A quantity of 80 μL crosslinker was added whilst the geometry was spinning at 7 rad s^{-1} during 7 s. Immediately after this mixing procedure, a 60-min time sweep recording of torsion analysis commenced. The oscillation strain amplitude was 0.75% at an oscillation frequency of 0.75 Hz. For each experiment, the measurement duration was limited to 1 hour.

3.5 Processing

All brightness-mode video clips were converted to still frames. A total number of 8109 frames was processed. For each imaging line in each brightness-mode image, the change in distal well surface was determined by automatically selecting the distal peak amplitude and converting the corresponding perceived distance to speed of sound, knowing the true unchanging distances to both well surfaces.

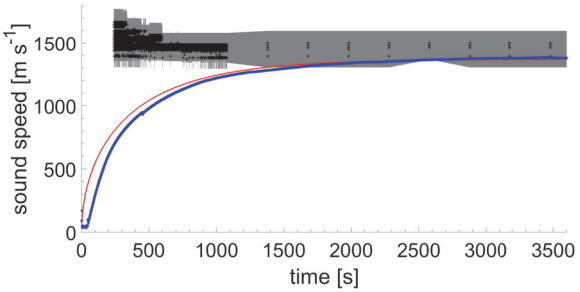

Fig. 4: Perceived speed of sound of gellan gum as a function of gelation time, measured from brightness-mode ultrasonic images (black with grey error bars), perceived from torsion rheometry (blue), and simulated from rheometry input (red).

For each rheometry measurement, the dynamic modulus magnitude was computed from the storage and loss moduli. From (5) followed the perceived speed of sound, presuming a constant hydrogel density of 8×10^2 kg m^{-3}.

The respective moduli and the time-dependent speed of sound in (1)–(6) were simulated using MATLAB® (The MathWorks, Inc., Natick, MA, USA). The rheometry data at $t = 3600$ s were used as first input parameters, after which curve matching was done manually.

4 Results and discussion

Figure 3 shows brightness-mode images of gelating gellan gum inside the cuboid well at selected times. For comparison, a frame has been added of the same well filled with prepared water. In all four frames, critical refraction artefacts were appreciated from the sides of the well perpendicular to the ultrasound probe [19]. Immediately after filling the well with gellan gum, speckle was observed from inside the well. This can be attributed to the presence of microbubbles entrapped in the hydrogel as a result of pouring. Although gas presence would lessen the speed of sound in a medium, the speed of sound of gellan gum was initially higher than the speed of sound in prepared water, as observed from the lower perceived distance to the distal reflector. The distal reflector was perceived to shift farther away from the proximal reflector over time. This indicates that the speed of sound of gellan gum became less during gelation. After one hour, the distal reflector was perceived to be at the position of the control. This indicates that the speed of sound after gelation had become the same as that of prepared water.

On overview of the speed-of-sound data collected from brightness-mode images and rheometry is demonstrated in Figure 4. In addition, a simulation curve has been added based on the simulation parameters $E_1 = 0.50\,\mathrm{GPa}$, $\frac{E_2}{\eta} = 1.7 \times 10^{-3}\,\mathrm{Hz}$, and $\eta\omega = 20\,\mathrm{MPa}$. The brightness-mode measurements had an inaccuracy of more than 10%. The measured speed of sound was not observed to change notably after 1000 s. The speed of sound measured from the brightness-mode images appeared to drop from $1542\pm211\,\mathrm{m\,s^{-1}}$ at 240 s to $1481\pm176\,\mathrm{m\,s^{-1}}$ after 3600 s. The perceived speed of sound computed from the rheometry data was computed to have risen to $1379\,\mathrm{m\,s^{-1}}$ after 3600 s, a value 92.5% of the mean speed of sound, but within the standard deviation of the brightness-mode measurement. From the storage and loss modulus data (not shown), it was confirmed that the gelation process was not yet complete, as both moduli were still gradually increasing.

5 Conclusion

In this study, we demonstrated the feasibility of using rheometry input for modelling and estimating the speed of sound during the gelation of gellan gum. The instantaneous speed of sound measured with brightness-mode ultrasound was observed to range from $1542\pm211\,\mathrm{m\,s^{-1}}$ to $1481\pm176\,\mathrm{m\,s^{-1}}$ during one hour. For this specific hydrogel, the speed of sound could be simulated from the dynamic modulus magnitude. The perceived value after one hour was 7.5% less than the mean speed of sound measured from brightness-mode images, but within a standard deviation thereof. It is noted that the gelation process was yet incomplete after one hour.

Author statement

Research funding: This work has been supported by the National Research Foundation of South Africa, Grant Number 127102, and by the Academy of Finland, Grant Numbers 336663 and 340026. Conflict of interest: Authors state no conflict of interest. Informed consent: Authors state that informed consent is not applicable. Ethical approval: Authors state that no ethical approval was required for this research as no human or animal samples or data were used.

References

[1] Weng L, Chen X, Chen W. Rheological characterization of in situ crosslinkable hydrogels dormulated from oxidized dextran and *N*-carboxyethyl chitosan. Biomacromolecules 2007;8:1109–1115.

[2] Koivisto JT, Gering C, Karvinen J, Cherian RM, Belay B, Hyttinen J, et al. Mechanically biomimetic gelatin–gellan gum hydrogeld for 3D culture of beating human cardiomycytes. ACS Appl Mater Interfaces 2019;11:20589–20602.

[3] Carlson CS, Deroubaix A, Penny C, Postema M. On the attenuation of pure black tattoo ink. SAIEE Afr Res J 2021;112:24–31.

[4] Brzozowski P, Penev KI, Mequanint K. Gellan gum gel tissue phantoms and gel dosimeters with tunable electrical, mechanical and dosimetric properties. Int J Biol Macromol 2021;180:332–328.

[5] Koivisto JT, Joki T, Parraga JE, Pääkönen R, Ylä-Outinen L, Salonen L, et al. Bioamine-crosslinked gellan gum hydrogel for neural tissue engineering. Biomed Mater 2017;12:025014.

[6] Ferris CJ, Stevens LR, Gilmore KJ, Mume E, Greguric I, Kirchmajer DM, et al. Peptide modification of purified gellan gum. J Mater Chem B 2015;3:1106–1115.

[7] Gering C, Koivisto JT, Parraga J, Leppiniemi J, Vuornos K, Hytönen VP, et al. Design of modular gellan gum hydrogel functionalized with avidin and biotinylated adhesive ligands for cell culture applications. PLoS ONE 2019;14:e0221931.

[8] Vuornos K, Huhtala H, Kääriäinen M, Hupa L, Kellomäki M, Miettinen S. Bioactive glass ions for in vitro osteogenesis and microvascularization in gellan gum-collagen hydrogels. J Biomed Mater Res B 2020;108:1332–1342.

[9] Chouhan G, Moakes RJA, Esmaeili M, Hill LJ, deCogan F, Hardwicke J, et al. A self-healing hydrogel eye drop for the sustained delivery of decorin to prevent corneal scarring. Biomaterials 2019;210:41–50.

[10] Douglas TEL, Schietse J, Zima A, Gorodzha S, Parakhonskiy BV, KhaleNkow D, et al. Novel self-gelling injectable hydrogel/alpha-tricalcium phosphate composites for bone regeneration: physiochemical and microcomputer tomographical characterization. J Biomed Mater Res A 2018;106A:822–828.

[11] Morris EP, Nishinari K, Rinaudo M. Gelation of gellan: a review. Food Hydrocoll 2012;28:373–411.

[12] Ahmed EM. Hydrogel: preparation, characterization, and applications: a review. J Adv Res 2015;6:105–121.

[13] Gibaud T, Dagès N, Lidon P, Jung G, Ahouré LC, Sztucki M, et al. Rheoacoustic gels: tuning mechanical and flow properties of colloidal gels with ultrasonic vibrations. Phys Rev X 2020;10:011028.

[14] Santos PHS, Carignano MA, Campanella O. Effect of shear history on rheology of time-dependent colloidal silica gels. Gels 2017;3:45.

[15] Menard KP. Dynamic Mechanical Analysis: A Practical Introduction. 2nd ed. Boca Raton: CRC; 2008.

[16] Mattei G, Ludovica Cacopardo L, Ahluwalia A. Engineering gels with time-evolving viscoelasticity. Materials 2020;13:438.

[17] van Otterloo J, Cruden AR. Rheology of pig skin gelatine: defining the elastic domain and its thermal and mechanical properties for geological analogue experiment applications. Tectonophysics 2016;683:86–97.

[18] Attenborough K, Postema M. A pocket-sized introduction to acoustics. Kingston upon Hull: University of Hull; 2008.

[19] Carlson CS, Postema M. Deep impact of superficial skin inking: acoustic analysis of underlying tissue. BIO Int 2021;2:109–120.